Real-Time Observation of Molecular Spinning with Angular High-Harmonic Spectroscopy

Lixin He,[1] Pengfei Lan,[1,*] Anh-Thu Le,[2] Baoning Wang,[1] Bincheng Wang,[1] Xiaosong Zhu,[1] Peixiang Lu,[1,3,†] and C. D. Lin[2]

[1]*Wuhan National Laboratory for Optoelectronics and School of Physics, Huazhong University of Science and Technology, Wuhan 430074, China*

[2]*Department of Physics, Cardwell Hall, Kansas State University, Manhattan, Kansas 66506, USA*

[3]*Laboratory of Optical Information Technology, Wuhan Institute of Technology, Wuhan 430205, China*

(Received 1 June 2018; revised manuscript received 14 September 2018; published 15 October 2018)

We demonstrate an angular high-harmonic spectroscopy method to probe the spinning dynamics of a molecular rotation wave packet in real time. With the excitation of two time-delayed, polarization-skewed pump pulses, the molecular ensemble is impulsively kicked to rotate unidirectionally, which is subsequently irradiated by another delayed probe pulse for high-order harmonic generation (HHG). The spatiotemporal evolution of the molecular rotation wave packet is visualized from the time-dependent angular distributions of the HHG yields and frequency shift measured at various polarization directions and time delays of the probe pulse. The observed frequency shift in HHG is demonstrated to arise from the nonadiabatic effect induced by molecular spinning. Different from the previous spectroscopic and Coulomb explosion imaging techniques, the angular high-harmonic spectroscopy method can reveal additionally the electronic structure and multiple orbitals of the sampled molecule. All the experimental findings are well reproduced by numerical simulations. Further extension of this method would provide a powerful tool for probing complex polyatomic molecules with HHG spectroscopy.

DOI: 10.1103/PhysRevLett.121.163201

Similar to a mechanical rotor, molecules can be forced to rotate around an axis by applying a torque. In the past few years, there has been a growing interest in utilizing short laser pulses to achieve molecular rotation with a preferred direction, which is called molecular unidirectional rotation (UDR) or molecular spinning. By coherently manipulating the rotational wave packet (RWP) with ultrashort lasers, molecular UDR has been created in experiment via adiabatic excitation with an optical centrifuge [1–4], nonadiabatic excitation with two sequential laser pulses [5–8], a chiral pulse train [9–11], or a polarization-shaped laser [12]. The ultrafast molecular UDR is expected to have a great impact on the formation of gas vortices [13], modification of molecule-surface scattering [14,15], and deflection of molecular polarization [16–18], etc. To understand these phenomena as well as facilitate further exploration of new applications, direct observation of the real-time evolution of the molecular RWP is essential.

Recently, several schemes have been reported to gain insight of molecular UDR. For example, the direction of molecular UDR can be effectively identified via spectroscopic observations of the rotational Doppler shift [7,8], or by the polarization-controlled Raman spectra [4]. Nevertheless, such spectroscopic measurements either lack temporal resolution [4], or require a strong anisotropic molecular distribution [7,8], making it difficult for observing its temporal evolution. Very recently, Lin *et al.* [19] first reported the experiment of visualizing molecular UDR in strong-field Coulomb explosion imaging (CEI), where the evolution of the molecular RWP is characterized by analyzing the momentum distribution of the fragment ions. It provides a profound view on the molecular spinning dynamics and has attracted wide attention [20–22]. Besides CEI, it is well known that laser-driven high-order harmonic generation (HHG) encodes rich information of molecular structure and dynamics [23–29]; thus high-harmonic spectroscopy (HHS) provides an alternative approach for probing molecular dynamics.

In this Letter, we demonstrate an angular HHS method to probe the molecular UDR. It offers the advantage of probing electron dynamics and nuclear dynamics from attosecond to picosecond timescales [30,31]. In our experiment, a double-pulse excitation scheme is utilized to create the molecular UDR. The spatiotemporal evolution of molecular RWP is visualized by probing the time-dependent angular distributions (ADs) of HHG yields at various polarization directions and time delays of the probe pulse. Moreover, due to the correlation of HHG and molecular UDR, HHG from the spinning N_2 shows obvious nonadiabatic frequency shift at the rotation revivals. The spinning dynamics of molecular RWP can also be revealed from the angle-dependent frequency shift of HHG. Besides, the harmonic ADs also reveal the electronic structure of the sample molecules. For example, for N_2, the two highest-occupied molecular

orbitals, HOMO and HOMO-1, both contribute to the HHG spectra.

In our experiment, we use two time-delayed, polarization-skewed pump pulses P_1 and P_2 to create molecular UDR and another linearly polarized probe pulse is focused on the UDR molecules to generate high-order harmonics [32]. To monitor the spatial distribution of the molecular RWP, we measure the ADs of HHG by scanning the polarizing angle α of the probe pulse with respect to P_1 in the UDR plane (i.e., the xz plane, see the geometry in [32]). Repeating this process for various time delays of the probe pulse, we can then experimentally characterize the spatio-temporal evolution of the molecular RWP via the time-dependent ADs of HHG. In Fig. 1, we show the experimental results of N_2 molecules. Figure 1(a) displays the time-dependent ADs of the 21st harmonic (H21) measured in the absence of P_2. Impulsively excited by the pump pulse P_1, the molecules are temporarily well aligned in a narrow cone around the x axis. The aligned RWP evolves under the field-free condition, and recurrence of alignment or antialignment appears at the rotational revivals as can be seen around $\tau = 8.4$ ps ($1T_{\mathrm{rev}}$, T_{rev} is the revival period) and 12.6 ps ($1.5T_{\mathrm{rev}}$) in Fig. 1(a). During the evolution, the aligned wave packet and therefore the ADs of the harmonics are always mirror symmetric with respect to the polarization direction of P_1, i.e., $\alpha = 0°$ or 180°. Next, we apply the polarization-skewed pump pulse P_2 at the time delay of $\tau = 4.05$ ps (near the half revival) where the molecules are maximally aligned. As shown in Fig. 1(b), the symmetrical alignment wave packet is driven by the torque induced by P_2, and turns to rotate unidirectionally. As a consequence, the measured time-dependent ADs of HHG exhibit a series of diagonal stripes at the rotational revivals.

To explain the experimental results, we next simulate the time-dependent ADs of HHG of UDR molecules. HHG

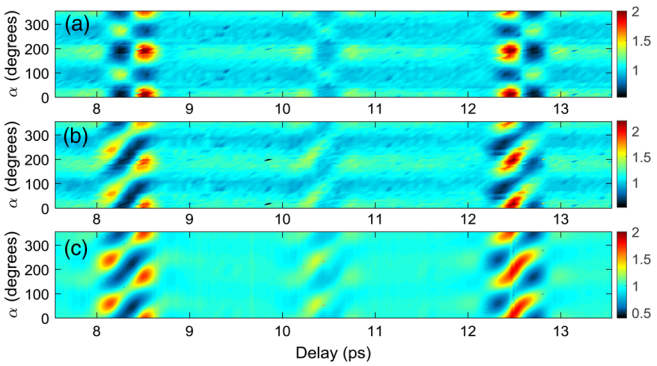

FIG. 1. (a) Angular distribution of H21 from N_2 as a function of the time delay of the probe pulse measured with the molecules excited by only the pump pulse P_1 (the case of alignment). (b) Same as (a), but for the molecules excited by both pump pulses, P_1 and P_2 (the case of UDR). (c) Theoretical simulation of the measured angular distribution of H21 in (b).

from the rotational molecular ensemble is a coherent superposition of the emission from molecules aligned at different angles. Molecules aligned at different angles are weighted by the instantaneous molecular axis distribution (MAD), i.e., the modulus square of the molecular RWP. Since molecular rotation is much slower than the HHG process, molecular rotation during the probe pulse for HHG is usually neglected [36–38]. In this case, HHG at each pump-probe time delay can be simulated with a fixed MAD. The time-dependent harmonic ADs $\mathcal{S}_q(\alpha,\tau)$ is then given by (for details, see Ref. [32])

$$\mathcal{S}_q(\alpha,\tau) = \left| \int_{\phi=0}^{\pi} \int_{\theta=0}^{2\pi} S_q(\theta')\rho(\theta,\phi,\tau) \sin\phi d\phi d\theta \right|^2. \quad (1)$$

Here, θ and ϕ are the polar and azimuthal angles of molecular axis with respect to the y and x axes. $\rho(\theta,\phi,\tau)$ is the MAD at the time delay τ, which is obtained by solving the time-dependent Schrödinger equation of the molecular RWP [20,22,39]. $S_q(\theta')$ is the angle-dependent induced dipole moment of the qth harmonic related to the single molecule response. θ' is the angle between the molecular axis and the polarization of the probe laser, which is given by $\cos\theta' = \sin\theta\cos\phi\cos\alpha + \sin\theta\sin\phi\sin\alpha = \sin\theta\cos(\alpha-\phi)$. According to Eq. (1), one can see that molecular UDR will change the MAD $\rho(\theta,\phi)$ and therefore the harmonic ADs $\mathcal{S}_q(\alpha,\tau)$, which leads to a synchronous evolution of the harmonic ADs and molecular RWP. Consequently, one can directly visualize the molecular UDR from the time-dependent harmonic ADs. Figure 1(c) shows the simulated result of H21 from the HOMO of N_2, which reproduces well the experimental observation in Fig. 1(b). Note that, in Fig. 1(c), the single-molecule response $S_q(\theta')$ is calculated with the quantitative rescattering (QRS) theory [38]. We have also performed the simulation with the strong-field approximation (SFA) model [40]. The SFA simulation is also consistent with the experimental result in Fig. 1(b).

Next, we show the detailed evolution of the measured ADs of HHG from N_2. Figures 2(f)–2(j) display the results of H21 at the time delays of $\tau = 8.15$, 8.25, 8.4, 8.6, and 8.7 ps, respectively. It is obvious that the harmonic AD rotates counterclockwise and varies from antialigned to aligned, and then to isotropic. Correspondingly, the simulated 3D-RWP illustrated in Figs. 2(a)–2(e) evolve from oblate to prolate, and then finally to near a sphere, in good agreement with the experimental H21 observation. Strictly speaking, the measured molecular RWP still requires a deconvolution of the ADs of HHG according to Eq. (1) [37]. However, HHG from the HOMO (σ_g symmetry) of N_2 is most pronounced when the laser is parallel to the molecular axis [32]. As a consequence, by scanning the polarization angle of the probe pulse, the obtained ADs of H21 is very close to the MAD (i.e., the projection of 3D-RWP) in the xz plane. Thus, the H21 data provide a

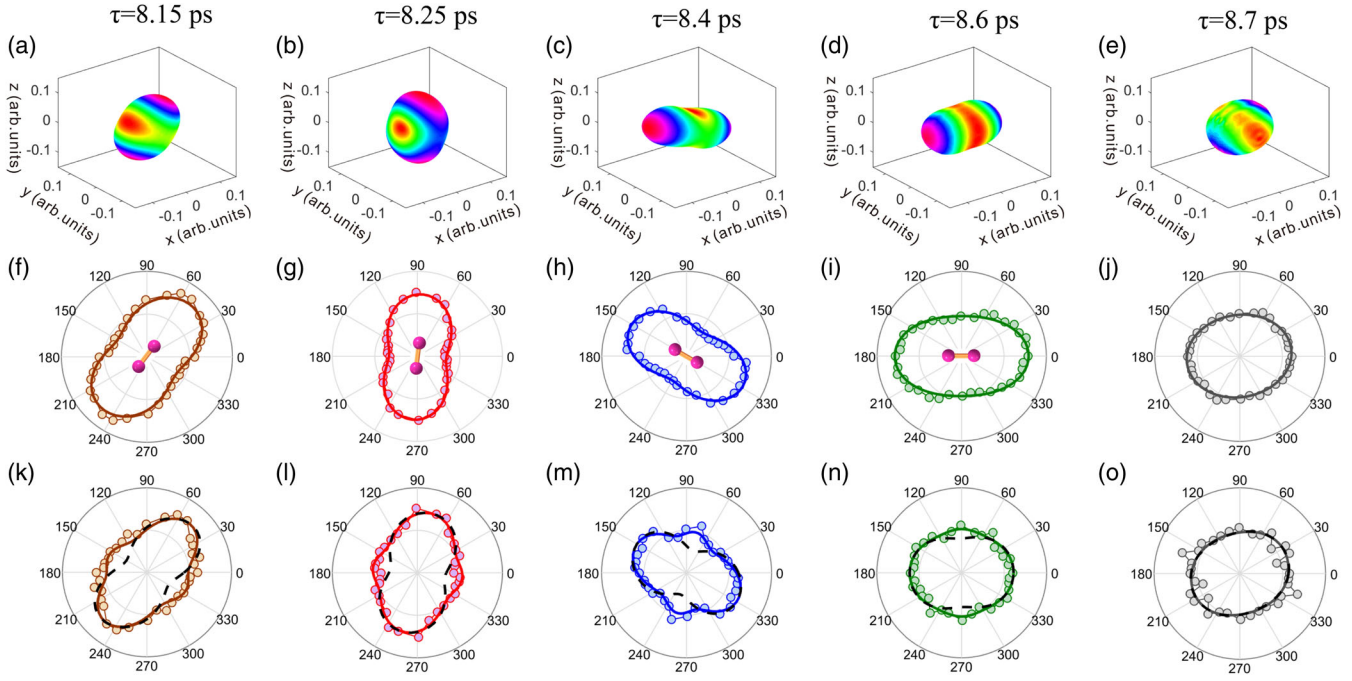

FIG. 2. (a)–(e) Simulated RWP distributions of N_2 at $\tau = 8.15$, 8.25, 8.4, 8.6, and 8.7 ps. (f)–(j) Polar plots of the ADs of H21 (circles) measured at the time delays in (a)–(e). Solid lines are the theoretical results simulated with only the HOMO contribution. (k)–(o) Same as (f)–(j), but for H33. Solid lines are theoretical results simulated with contributions of both the HOMO and HOMO-1. Dashed lines are those with only the HOMO contribution.

direct visualization of the molecular UDR in both time and space (see movie in the Supplemental Material [32]). We note that all harmonics below H27 show the same agreement. Quantitatively, the MAD can be retrieved by deconvolution of the harmonic ADs under certain approximations, in a similar fashion as was done by Ren *et al.* [41] in their retrieval of the angle-dependent photoionization cross section of N_2 from HHG spectra. Other similar schemes also exist [42–44].

Our experiment also obtained the ADs of higher harmonics near the cutoff, e.g., H33. It has a different structure compared to harmonics in the plateau region. As depicted in Figs. 2(k)–2(o), one can still identify the counterclockwise rotation from the temporal evolution of the ADs of H33. However, the spatial distribution of H33 shows a considerable "fatter" waist where the probe laser is nearly perpendicular to the major axis of the MAD. To explain these observations, we have performed simulations for H21 and H33 of N_2 for the MADs in Figs. 2(a)–2(e). The results are shown as solid lines in Figs. 2(f)–2(o). Here, both the measured and simulated harmonic signals have been normalized by the harmonics in the isotropic case for better comparison. With only the contribution of HOMO of N_2, the experimental results of H21 are well reproduced [see solid lines in Figs. 2(f)–2(j)]. For H33, it shows a clear difference at the waist between the simulation and experiment [see dashed lines in Figs. 2(k)–2(o)]. To explain this difference, we have performed further simulations by including the HOMO-1 contribution in Figs. 2(k)–2(o) (solid lines). Because of its π_g symmetry, HHG from the HOMO-1 of N_2 is most prominent when the laser is perpendicular to the molecular axis [45,46]. Its contribution is responsible for the "fatter" waist seen in Figs. 2(k)–2(o). We also note that the HOMO-1 contribution is small for low photon energies [32], and will not affect the ADs of harmonics below H27 seriously. This is consistent with previous studies [45,46].

We have also carried out the experiment on UDR CO_2 molecules to compare with the results from N_2. In this case, the 45° polarized pump pulse P_2 is applied at the maximum alignment near the half revival ($\tau = 21.4$ ps). Figures 3(f)–3(o) show the time-dependent ADs of H25 and H35 measured near the full revival of CO_2. Figures 3(a)–3(e) are the 3D-RWP obtained from numerical simulations. It is evident that the harmonic ADs rotate counterclockwise as the RWP. However, unlike N_2, the ADs of the harmonics in CO_2 peak mainly along the direction perpendicular to the main axis of the MAD in the xz plane. The difference is that the HOMO of CO_2 has the π_u symmetry, while for N_2, the HOMO has the σ_g symmetry. This leads to a maximum of the single-molecule HHG yield at a large alignment angle (the angle between the polarization direction of the driving laser and the molecular axis) around 70° [32,38,47]. In this case, the spatial distribution of molecular RWP can be retrieved by performing a deconvolution of the harmonic ADs with the rotational coherence spectroscopy method [44]. In addition, we found that harmonics of CO_2 near the cutoff (e.g., H35) show much more irregular ADs. Our

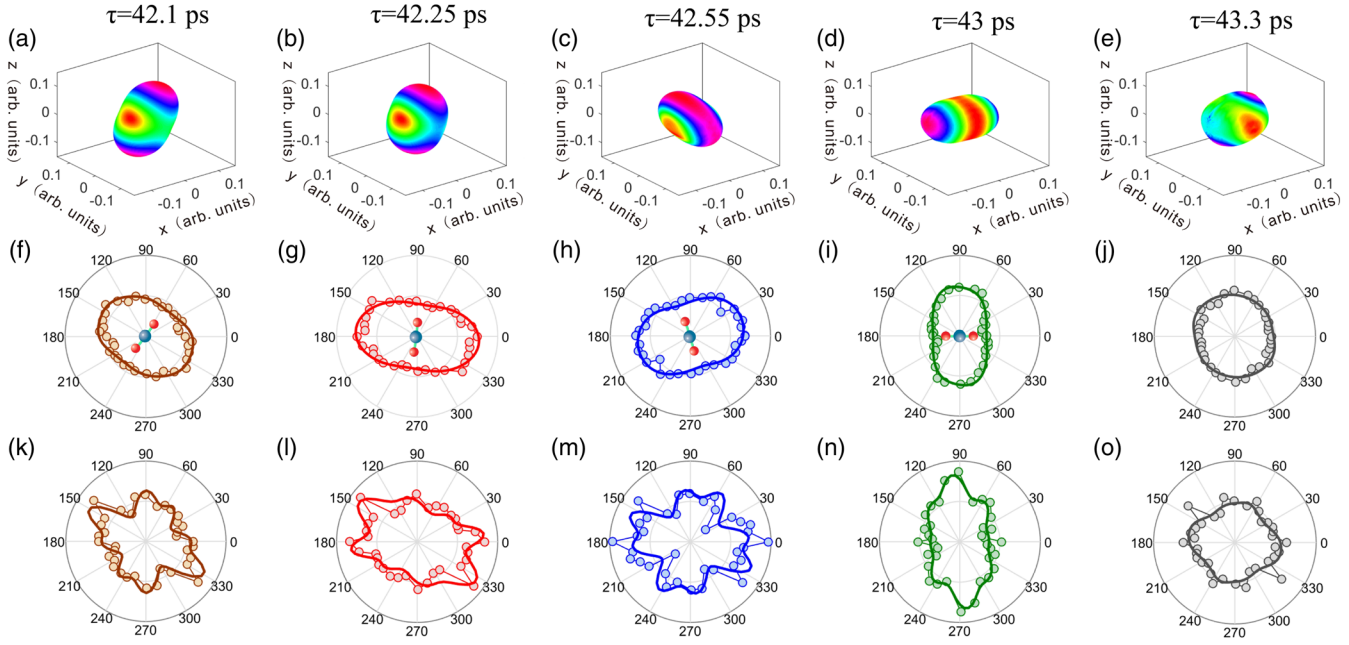

FIG. 3. (a)–(e) Simulated RWP distributions of CO_2 at $\tau = 42.1$, 42.25, 42.55, 43, and 43.3 ps. (f)–(j) Polar plots of the ADs of H25 (circles) measured at the time delays in (a)–(e). Solid lines are the theoretical results simulated with the HOMO contribution. (k)–(o) Same as (f)–(j), but for H35.

simulations based on the QRS theory [solid lines in Figs. 3(f)–3(o)] indicate that these abnormal-looking harmonic ADs are mainly due to the double-humped alignment-dependent photoionization cross section (PICS) of the HOMO of CO_2 [32,38,47], which complicate considerably the AD of $S_q(\theta')$ and therefore that of $\mathcal{S}_q(\alpha)$. We have also performed simulations with the standard SFA model. The SFA does not reproduce the experiment due to the incorrect PICS. Note that a multiple orbitals effect has also been reported for CO_2 to explain the harmonic structures in the cutoff region [48,49]. In our simulations, the HOMO of CO_2 alone is able to well reproduce the experimental results. The difference in the interpretation is likely due to the accuracy of PICS used in the theory. In Refs. [38,47], accurate transition dipoles from state-of-the-art molecular photoionization calculations were used in the QRS. The PICS from these calculations have been found to be in good agreement with conventional photoionization experiments. By comparing Fig. 3 to Fig. 2, one can see that the harmonic ADs depend sensitively on the molecular structure. For molecules under the same MAD [e.g., in Figs. 2(d) and Fig. 3(d)], the difference in harmonic ADs provides a clear signature for differentiating the orbital structures of the spinning molecules that is not attainable by previous spectroscopic and CEI methods.

Our experiment also demonstrated a frequency shift in HHG from UDR molecules. Figures 4(a)–4(b) show the measured frequency shift ($\Delta\lambda$) of H17 (squares) from the aligned and UDR N_2 as a function of the pump-probe delay at various α. One can see that H17 from UDR N_2 is blueshifted (or redshifted) at the rotation revivals. Moreover, the frequency shift at the revivals shows diagonal stripes similar to that of the harmonic ADs in Fig. 1(b), from which the molecular UDR can also be visualized. This frequency shift is also observed in HHG from aligned N_2 [Fig. 4(a)], which, however, shows a mirror-symmetric distribution like that in Fig. 1(a). Note that such a frequency shift cannot be reproduced by the commonly used fixed-MAD approximation. To explain the UDR results, we have modified the theoretical model by taking molecular UDR during the probe pulse into account (see Ref. [32]). As shown in Fig. 4(c), which presents the results of $\alpha = 0°$, the simulated results (solid line) agree well with the experimental observations. Our simulations indicate that the frequency shift in HHG mainly arises from molecular UDR

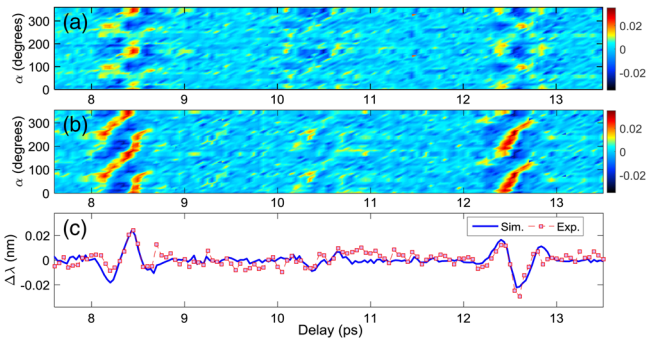

FIG. 4. (a) Time-dependent frequency shift $\Delta\lambda$ of H17 from aligned N_2 measured at various α. (b) Same to (a), but for the spinning N_2. (c) is the result of $\alpha = 0°$ in (b). Squares and solid line correspond to the measured and calculated results, respectively.

during the probe pulse, which leads to a difference in the alignment degrees of molecules (anisotropy of MAD) at the leading and trailing edges of the probe pulse [32] and then breaks the symmetry of harmonic emission during the probe pulse. Furthermore, due to the nonadiabatic effect of the time-dependent laser intensity [50–52], HHG dominated at the leading or trailing edge emerges a blueshift or redshift as observed in our experiment. In contrast to UDR, the evolution of aligned RWP also causes the asymmetry of MAD at the leading and trailing edges of the probe pulse. Therefore, HHG from aligned N_2 also shows the frequency shift at the alignment revivals. However, like the harmonic ADs in Fig. 1(a), the frequency shift of HHG from aligned N_2 is also symmetrically distributed due to the spatial symmetry of the aligned RWP. It is expected that the nonadiabatic frequency shift in Fig. 4 will decrease with increasing harmonic order, since higher-order harmonic emission occurs within a narrow time interval closer to the peak of the laser field, where the variation of MAD is smaller and the nonadiabatic effect is weaker. The observed frequency shift is a new effect arising from the correlation of molecular rotation and HHG, which has never been reported before. Our simulations based on the modified model suggest that the rotational nonadiabatic effect will not modify the harmonic ADs discussed above. Moreover, the nonadiabatic frequency shift is less obvious for CO_2 molecules due to its much slower rotation.

In summary, an angle-dependent HHS method was used to measure the evolution of molecular RWP in both time and space. By using a double-pulse scheme, unidirectional rotation of molecules is created for N_2 and CO_2 molecules. Through their subsequent interaction with a probe pulse, we have measured the angle dependence of HHG from these UDR molecules at various time delays. For N_2, we showed that the MAD of the spinning molecules can be directly retrieved from the measured angle-dependent yields for harmonics below the cutoff. A multiple orbitals effect has also been revealed by the ADs of harmonics near the cutoff. Moreover, a new nonadiabatic frequency shift is observed in HHG from N_2. From the angle-dependent frequency shift, the molecular UDR can also be identified. While for CO_2 molecules, the harmonic ADs are markedly different from that of N_2. A more general deconvolution scheme may be needed for the retrieval of the RWP. The advantage of the current approach is that the HHG spectra can also be investigated in addition to the UDR. Different harmonics can offer a consistency check for the retrieved UDR. In the future, this may prove to be a more powerful tool for studying HHG from polyatomic molecules for which strong alignment or orientation is difficult. In particular, by varying the time delay of the second pump pulse, one can enhance or reduce the contribution from the different molecular alignments in HHG spectra. The possibility of probing HHG from many directions of UDR molecules may provide an ample set of HHG data for extracting the complex electron structure of polyatomic molecule.

The authors gratefully acknowledge Xu Wang for helpful discussions. This work was supported by the National Natural Science Foundation of China under Grants No. 11627809, No. 11874165, No. 11704137, and No. 11774109. A. T. L. and C. D. L. were partially supported by the U.S. Department of Energy under Grant No. DE-FG02-86ER13491.

*pengfeilan@hust.edu.cn
†lupeixiang@hust.edu.cn

[1] J. Karczmarek, J. Wright, P. Corkum, and M. Ivanov, Phys. Rev. Lett. **82**, 3420 (1999).
[2] D. M. Villeneuve, S. A. Aseyev, P. Dietrich, M. Spanner, M. Yu. Ivanov, and P. B. Corkum, Phys. Rev. Lett. **85**, 542 (2000).
[3] L. Yuan, S. W. Teitelbaum, A. Robinson, and A. S. Mullin, Proc. Natl. Acad. Sci. U.S.A. **108**, 6872 (2011).
[4] A. Korobenko, A. A. Milner, and V. Milner, Phys. Rev. Lett. **112**, 113004 (2014).
[5] S. Fleischer, Y. Khodorkovsky, Y. Prior, and I. Sh. Averbukh, New J. Phys. **11**, 105039 (2009).
[6] K. Kitano, H. Hasegawa, and Y. Ohshima, Phys. Rev. Lett. **103**, 223002 (2009).
[7] O. Korech, U. Steinitz, R. J. Gordon, I. S. Averbukh, and Y. Prior, Nat. Photonics **7**, 711 (2013).
[8] U. Steinitz, Y. Prior, and I. S. Averbukh, Phys. Rev. Lett. **112**, 013004 (2014).
[9] S. Zhdanovich, A. A. Milner, C. Bloomquist, J. Floß, I. Sh. Averbukh, J. W. Hepburn, and V. Milner, Phys. Rev. Lett. **107**, 243004 (2011).
[10] C. Bloomquist, S. Zhdanovich, A. Milner, and V. Milner, Phys. Rev. A **86**, 063413 (2012).
[11] J. Floß and I. Sh. Averbukh, Phys. Rev. A **86**, 063414 (2012).
[12] G. Karras, M. Ndong, E. Hertz, D. Sugny, F. Billard, B. Lavorel, and O. Faucher, Phys. Rev. Lett. **114**, 103001 (2015).
[13] U. Steinitz, Y. Prior, and I. Sh. Averbukh, Phys. Rev. Lett. **109**, 033001 (2012).
[14] D. Shreenivas, A. Lee, N. Walter, D. Sampayo, S. Bennett, and T. Seideman, J. Phys. Chem. A **114**, 5674 (2010).
[15] Y. Khodorkovsky, J. R. Manson, and I. Sh. Averbukh, Phys. Rev. A **84**, 053420 (2011).
[16] S. M. Purcell and P. F. Barker, Phys. Rev. Lett. **103**, 153001 (2009).
[17] E. Gershnabel and I. Sh. Averbukh, Phys. Rev. Lett. **104**, 153001 (2010).
[18] E. Gershnabel and I. Sh. Averbukh, Phys. Rev. A **82**, 033401 (2010).
[19] K. Lin, Q. Song, X. Gong, Q. Ji, H. Pan, J. Ding, H. Zeng, and J. Wu, Phys. Rev. A **92**, 013410 (2015).
[20] K. Mizuse, K. Kitano, H. Hasegawa, and Y. Ohshima, Sci. Adv. **1**, e1400185 (2015).
[21] A. Korobenko, J. W. Hepburn, and V. Milner, Phys. Chem. Chem. Phys. **17**, 951 (2015).

[22] K. Lin *et al.*, Phys. Rev. X **6**, 041056 (2016).
[23] J. Itatani, J. Levesque, D. Zeidler, H. Niikura, H. Pépin, J. C. Kieffer, P. B. Corkum, and D. M. Villeneuve, Nature (London) **432**, 867 (2004).
[24] S. Haessler *et al.*, Nat. Phys. **6**, 200 (2010).
[25] P. M. Kraus, A. Rupenyan, and H. J. Wörner, Phys. Rev. Lett. **109**, 233903 (2012).
[26] E. Frumker *et al.*, Phys. Rev. Lett. **109**, 249902(E) (2012).
[27] S. Baker, J. S. Robinson, C. A. Haworth, H. Teng, R. A. Smith, C. C. Chirila, M. Lein, J. W. G. Tisch, and J. P. Marangos, Science **312**, 424 (2006).
[28] P. Lan *et al.*, Phys. Rev. Lett. **119**, 033201 (2017).
[29] L. He *et al.*, Nat. Commun. **9**, 1108 (2018).
[30] J. Wu *et al.*, Phys. Rev. Lett. **111**, 023002 (2013).
[31] P. F. Lu *et al.*, Proc. Natl. Acad. Sci. U.S.A. **115**, 2049 (2018).
[32] See Supplemental Material at for http://link.aps.org/supplemental/10.1103/PhysRevLett.121.163201, which includes Refs. [33–35], for the experimental and theoretical methods of high-harmonic generation from spinning molecules, and a movie illustrating the time-dependent angular distributions of H21 from spinning N_2 and the spatiotemporal evolution of the three-dimensional rotational wave packet.
[33] S. Saugout, E. Charron, and C. Cornaggia, Phys. Rev. A **77**, 023404 (2008).
[34] F. Brandi, F. Giammanco, and W. Ubachs, Phys. Rev. Lett. **96**, 123904 (2006).
[35] H. J. Shin, D. G. Lee, Y. H. Cha, K. H. Hong, and C. H. Nam, Phys. Rev. Lett. **83**, 2544 (1999).
[36] K. Yoshii, G. Miyaji, and K. Miyazaki, Opt. Lett. **34**, 1651 (2009).
[37] K. Yoshii, G. Miyaji, and K. Miyazaki, Phys. Rev. Lett. **106**, 013904 (2011).
[38] A.-T. Le, R. R. Lucchese, S. Tonzani, T. Morishita, and C. D. Lin, Phys. Rev. A **80**, 013401 (2009).
[39] H. Stapelfeldt and T. Seideman, Rev. Mod. Phys. **75**, 543 (2003).
[40] M. Lewenstein, P. Balcou, M. Y. Ivanov, A. L'Huillier, and P. B. Corkum, Phys. Rev. A **49**, 2117 (1994).
[41] X. Ren, V. Makhija, A.-T. Le, J. Tross, S. Mondal, C. Jin, V. Kumarappan, and C. Trallero-Herrero, Phys. Rev. A **88**, 043421 (2013).
[42] J. B. Bertrand, H. J. Wörner, P. Hockett, D. M. Villeneuve, and P. B. Corkum, Phys. Rev. Lett. **109**, 143001 (2012).
[43] A. Rupenyan, J. B. Bertrand, D. M. Villeneuve, and H. J. Wörner, Phys. Rev. Lett. **108**, 033903 (2012).
[44] X. Wang, A.-T. Le, Z. Zhou, H. Wei, and C. D. Lin, Phys. Rev. A **96**, 023424 (2017).
[45] B. K. McFarland, J. P. Farrell, P. H. Bucksbaum, and M. Gühr, Science **322**, 1232 (2008).
[46] A.-T. Le, R. R. Lucchese, and C. D. Lin, J. Phys. B **42**, 211001 (2009).
[47] C. D. Lin, A.-T. Le, Z. Chen, T. Morishita, and R. Lucchese, J. Phys. B **43**, 122001 (2010).
[48] O. Smirnova, Y. Mairesse, S. Patchkovskii, N. Dudovich, D Villeneuve, P. B. Corkum, and M. Ivanov, Nature (London) **460**, 972 (2009).
[49] O. Smirnova, S. Patchkovskii, Y. Mairesse, N. Dudovich, D. Villeneuve, P. Corkum, and M. Y. Ivanov, Phys. Rev. Lett. **102**, 063601 (2009).
[50] M. B. Gaarde, F. Salin, E. Constant, P. Balcou, K. J. Schafer, K. C. Kulander, and A. L'Huillier, Phys. Rev. A **59**, 1367 (1999).
[51] P. Salières, A. L'Huillier, P. Antoine, and M. Lewenstein, Adv. At. Mol. Opt. Phys. **41**, 83 (1999).
[52] C. M. Heyl, J. Gudde, U. Hofer, and A. L'Huillier, Phys. Rev. Lett. **107**, 033903 (2011).